

SYMPOSIUM ON COAL LIQUIDS UPGRADING

PRESENTED BEFORE
THE DIVISION OF FUEL CHEMISTRY, INC.
AMERICAN CHEMICAL SOCIETY
HOUSTON MEETING
MARCH 25-28, 1980

CATALYST DEACTIVATION IN HYDROTREATING
COAL-DERIVED LIQUIDS

R. Sivasubramanian,¹ J. H. Olson and J. R. Katzer*
Center for Catalytic Science and Technology
Department of Chemical Engineering
University of Delaware
Newark, Delaware 19711

¹Air Products and Chemicals, Inc.; P.O. Box 538, Allentown,
Pennsylvania 18105

*To whom correspondence should be addressed. (302) 738-8056

CATALYST DEACTIVATION IN HYDROTREATING COAL-DERIVED LIQUIDS

Introduction

Coal liquefaction processes are likely to be commercialized within the next decade. Coal-derived liquids contain larger fractions of heteroatoms (sulfur, nitrogen, oxygen) than petroleum liquids. Hydroprocessing of these liquids will become necessary to improve the quality of the products. Considerable work has been done in determining catalyst deactivation rates in petroleum hydroprocessing. However, coal-derived liquids differ considerably from petroleum liquids in their aromaticity, metals content and C/H ratio. Coal-derived liquids are much harder to hydroprocess, cause more rapid catalyst deactivation, and represent a step upward in terms of difficulty of hydrotreating.

Characterization studies on aged catalysts can provide an understanding of the causes for catalyst deactivation and may lead to optimum design of reactors and improved catalysts. Characterization of three different coal-liquefaction catalysts that have been in direct contact with coal have been performed earlier in this laboratory (1,2,3). However, in the present study a catalyst that had been used to hydrotreat a coal-derived liquid is characterized.

Experimental

Ni-Mo/Al₂O₃ catalyst samples were obtained from a laboratory-size trickle-bed reactor that was used to hydrotreat an equal

volume mixture of raw anthracene oil and sýnthoil liquid. The properties of this particular feedstock is given in Table I. The feed oil had a sulfur content of 0.54 wt %, a nitrogen content of 1.21 wt % and 1.05 wt % ash. Table II presents the operating conditions in the trickle-bed reactor for the particular run from which the catalyst samples were obtained. At the end of the run, the reactor was shut down and the reactor was cut into three different sections and catalyst samples were obtained from the top, middle and bottom sections of the reactor. The spent catalyst pellets from the three different sections were analyzed with a scanning electron microscope (SEM) equipped with an energy dispersive x-ray analyzer (EDAX) and with an electron microprobe. In addition spent catalysts were regenerated (coke burnt off) and the hydrodesulfurization (HDS) and hydrodenitrogenation (HDN) activities of the fresh, spent and regenerated catalysts were compared.

Microscopy Studies

Most of the catalyst samples used in the microscopy studies were prepared by sectioning the catalyst; mounting the catalyst in potting material on a SEM sample holder, and then grinding the exposed surface flat with various grits down to 0.25 μ diamond dust. The lapped samples then were carbon shadowed. These samples then were inspected in light microscopy, SEM and the electron microprobe.

The SEM with EDAX was used in two modes, first conventional inspection of the surface coupled with spot analyses of distinctive

features. The second mode was to scan the surface for specific elements. The microprobe was used in three modes, inspection of the surface elemental scans (these scans are superior to the EDAX elemental scans), and finally to find the elemental response along a 100 x 0.5 micron line parallel to a tangent to the catalyst surface. The line scan was mechanically driven to sweep an area near the catalyst exterior surface.

Samples also were then prepared by cleaving the catalyst, mounting on an SEM post and then removing surface "coke" by plasma etching. This preparation method reveals the distribution of mineral matter on the catalyst surface.

Activity Studies

In order to determine the activity decay of the spent catalysts, the spent catalysts were regenerated and the activities of the spent catalysts were compared with that of the fresh and regenerated catalysts for hydrodesulfurization and hydrodenitrogenation using a mixture of dibenzothiophene and quinoline dissolved in hexadecane as a feedstock in a batch autoclave reactor. Earlier experiments by Chiou and Olson (2,3) were done by crushing the spent pellets to 140 mesh. For this work, in order to find out the effect of crushing the spent catalysts, it was decided to conduct experiments using crushed particles as well as using the spent catalysts as received (8/10 mesh).

A mixture of spent catalysts from all three sections of the reactor was obtained and this mixture was divided into two halves.

One half of this mixture was ground to a size of 140 mesh. Both halves were regenerated by controlled combustion of the coke deposited on the catalyst. The regeneration process was done by passing a 2% oxygen in helium over the spent catalysts at a temperature of 450°C at a flow rate of 100 cc/min. The burning process was continued until the weight of residual catalyst became constant.

All the experiments were conducted in a 300 cc standard autoclave reactor (Autoclave Engineers, Erie, PA) equipped with a variable speed magnadrive; the autoclave was operated in batch mode. A special injection system was used to inject a slurry of catalyst, reactants and carbon disulfide in a small amount of carrier oil into the reactor after it had been stabilized at reaction temperature. This technique allowed the precise definition of zero time and eliminated complications including reaction and possible catalyst activity changes arising from long heat-up times. The system has been described elsewhere (4). However, the above technique could not be utilized in runs involving catalyst pellets. For these runs a special basket was designed that held the catalyst in place inside the autoclave reactor. For the pellet runs, the reactants and carbon disulfide in carrier oil were injected after the reactor had reached the operation temperature. Two blank runs not containing catalyst were made to determine the effect of reactor walls and the catalyst basket.

Table III presents the operating conditions for the batch autoclave reactor for all the runs used in this study. N-hexadecane

was used as a carrier oil. All catalysts were presulfided, and in order to maintain the catalyst in the sulfided form during the reaction, an amount of CS_2 equivalent to 0.05 wt % of the carrier oil was added to the injection tubing together with catalyst and reactants. Under the operating conditions carbon disulfide was rapidly converted to hydrogen sulfide and methane. The amount of CS_2 created 1.4% higher concentration of H_2S than that required to keep the catalyst in the sulfided form. Liquid samples were analyzed using a gas chromatograph equipped with a glass capillary column (OV101, 75 m).

Results of Microscopic Investigations

The prior part of this section presents a fairly detailed narrative of the SEM results for the sample taken from the top (nearest the entrance) of the reactor and then less complete descriptions for the data gathered for the middle and bottom samples. This is followed by a presentation of the results from the microprobe investigations and plasma etching. The various experimental methods yield a reasonably consistent description for the deposition of mineral matter and coke at the catalyst surface.

SEM - Top Sample

Figures 1A and B are conventional photo micrographs of the polished cross section of the catalyst pellet. These two figures show the deposition of an irregular crust about 75 microns thick around the entire exterior surface of the catalyst. In addition there is a thin region about 10 microns thick which

appears on about one-third of the catalyst. The catalyst also has many circular regions about 40 microns in diameter which appear distinct from the polished section of the catalyst. Finally the zone near the surface contains many cracks with a thickness of 1-5 microns. The roughness of the catalyst exterior surface suggests that a small portion of the catalyst may have spalled away. The smaller boxed area in Figure 1B corresponds to a zone which was examined with scanning electron microscopy. The larger rectangle corresponds to a zone evaluated with the electron microprobe analyzer.

Figure 2A shows the surface of the catalyst pellet as seen with a scanning electron microscope. In contrast to the light microscope, the outer crust is seen to contain many large (~1 micron) cracks. In addition the outer crust contains about 20 percent of small particles (~0.5 micron) embedded in an indistinct matrix. The inner crust also is seen to contain many voids and cracks; this zone appears to be made by aggregation of small crystals. The catalyst support contains a number of extended large cracks near the external surface. In addition there are a number of shallow depressions, 40 microns in the largest dimension which will be described more completely later. In summary the surface has two distinct crusts and a zone containing large fissures near the exterior surface.

Figure 2B is an aluminum area scan made by recording the aluminum signal from the EDAX. Figures 2B and 2A correspond.

There are three distinct zones for the aluminum signal, the upper zone for potting material, the middle zone for the crust, and the bottom zone of the catalyst support. Closer inspection reveals that the cracks seen clearly in the backscatter electron scan also appear, although less distinctly, in the aluminum scan. The aluminum scan shows that the inner and outer crust regions contain aluminum and that the catalyst exterior surface has been roughened in the process.

Figure 3A is a SEM-EDAX area scan for silicon. This scan shows that the exterior crust contains a high concentration of silicon; the gray (intermediate) zone on Figure 2B corresponds exactly with the bright zone of Figure 3A. In addition there is some penetration of silicon into the interior of the catalyst near the exterior surface. Careful examination of the crust region identifies a few zones (~15 microns across) of very high silicon concentration.

Figure 3B is a SEM-EDAX area scan for calcium. The calcium signal in the catalyst is only slightly greater than background, and therefore the zones are far less distinct. However the high-silicon region of Figure 3A has a corresponding but less distinct zone on the calcium scan. In addition, the major cracks appear faintly. Some zones of high silicon concentration in the crust region of Figure 3A appear as voids in the calcium scan on Figure 3B. Finally there is a small calcium signal in the catalyst support; however the calcium signal in the catalyst is barely above background.

Figure 4A, the SEM-EDAX Area Scan for Sulfur, and Figure 4B, the SEM-EDAX Area Scan for Iron, will be discussed together. The demarcation between the catalyst and the crust can be seen on both figures but is far clearer on the iron scan. The catalyst is sulfided, and therefore there should be a distinct sulfur signal in the interior of the catalyst. The cracks seen clearly on Figure 2A appear faintly on the sulfur area scan. The crust region gives a near-perfect correlation between the two signals. Further, the high section zones are seen as voids in the two figures. There is a fairly distinct zone of higher sulfur concentration in the crust located in the center of the figure which also appears, although less clearly, in the iron scan. Thus the exterior and the interior crusts contain an iron-sulfur compound. There is some penetration of iron into the catalyst, and sulfur appears throughout the catalyst interior.

Figure 5A is a titanium SEM-EDAX scan of the area. The interior crust region of Figure 2A is seen to contain a high concentration of titanium. In addition there is a significant concentration of titanium in the exterior crust. Finally there is some penetration of titanium into the near surface of the catalyst.

Figure 5B shows a molybdenum SEM-EDAX scan of the catalyst. Molybdenum is the major active element in the catalyst. The molybdenum signal correlates with the intense aluminum signal of Figure 2B. The cracks in the catalyst can be seen as voids in the molybdenum signal.

The area scanned in Figures 2A-5B were also examined for nickel and zinc. These scans gave no signal above background even though EDAX spot and line analyses showed that these elements are present. Indeed, the catalyst contains nickel as a hydrogenation promoter.

Figure 6A is an electron backscatter readout taken in the microprobe analyzer prior to making the line scans. This area appears as the large rectangle on Figure 1B. Consistent with Figure 2B, the figure shows an outer and inner crust, major cracks in the catalyst near the surface, and several flat depressions about 40 microns in diameter. The line in the crust region corresponds to the orientation of the 60 micron line scan used to find the average composition of the crust.

Figure 6B is the titanium microprobe area scan which corresponds to Figure 6B. The microprobe area scan for titanium is much more sensitive than the SEM-EDAX area scan, and therefore more details emerge: the inner crust is seen to produce a very high titanium signal. The dense exterior crust contains an intermediate concentration of titanium; however the crust in the upper left portion of the figure appears to be nearly free of titanium. The shallow craters and the cracks in the catalyst interior are decorated with titanium. Thus the titanium is distributed in a complex way throughout the crust region of the catalyst.

SEM - Middle Sample

Figures 7A and 7B are conventional micrographs of the polished section of a catalyst pellet taken from the middle of the reactor. Consistent with the top sample, there is an irregular crust about 75 microns thick which completely covers the catalyst. Likewise there is a thin inner crust which covers about one-quarter of the surface. Again the surface region of the catalyst has many fissures, and the spent catalyst has many ponds which have been decorated with process material. The rectangular region on Figure 7B locates the region examined more closely with the SEM-EDAX and the microprobe. The region was chosen because the thin crust is unusually flat there.

Figures 8A and 8B are the SEM inspections of the sectioned catalyst. Owing to the greater depth of field of the SEM than for the light microscope, the cracks and the round depressions of the surface can be seen more clearly. Figure 8B, taken at 800X corresponds to the region examined by SEM-EDAX area scans. The latter data are recorded in Figures 9A-11B.

In harmony with the top sample the exterior crust has a high silicon concentration (Figure 9A) and contains grains of extremely high silicon concentration. The silicon density in the third of the crust nearest to the surface is greater than for the outer two-thirds; this density variation also can be seen in the SEM micrographs. The calcium concentration (Figure 9B) is fairly

uniform in both the crust and the catalyst interior. There is more calcium in the crust than in the catalyst.

The sulfur (Figure 10A) and iron (Figure 10B) area scans show a very high correlation for these two elements in the crust, a very low concentration of iron in the catalyst, and an intermediate concentration of sulfur in the catalyst. These results are similar to the top sample.

The titanium scan (Figure 11A) shows a very high concentration of this element in the inner crust, a high concentration in the outer crust, and decoration of the two shallow depressions on Figure 8B with titanium. In addition the small piece of material sitting on the surface of the catalyst at the extreme left is high in titanium. This speck appears to be a piece of inner crust which may have been displaced during sample preparation.

Bottom Sample

Figures 12A and 12B are conventional photo micrographs of the sectioned and polished catalyst sample taken from the bottom of the reactor. The small square shown on Figure 12A is examined at higher magnification with SEM; the micrographs are given in Figures 14A and 14B. The large rectangle area in Figure 12B was given SEM-EDAX scans; the data are given on Figures 15A-17B.

The bottom sample is distinctly different from the top and middle samples. First, the cemented exterior crust does not cover the entire surface, but instead appears to have filled in

regions where the surface of the catalyst has spalled away. Second, there is no titanium-rich inner crust on the catalyst in all of the samples investigated.

Figures 13A and 13B show two magnifications of the catalyst area in a zone where crust has formed. The enhanced depth of the field shows very large cracks and several round, shallow pits in the catalyst support. These features of the bottom sample are identical to the other two samples.

Figures 14A and 14B are two pictures at 1000x of the small square identified on Figure 12A. These pictures show that the flat crater is filled with polycrystalline material smaller than 0.5 microns which is similar to the inner crust material. A spot EDAX analysis shows that this zone contains significant quantities of titanium.

The SEM-EDAX area scans for the bottom sample are shown in Figures 15A-17B. The results for the six elements Si, Ca, S, Fe, Ti and Mo are identical effectively to the middle sample with the following exceptions:

- a) there are no particles very high in sulfur in the crust,
- b) there is less difference between the sulfur concentration in the crust and in the catalyst,
- c) the titanium concentration in the outer crust is very distinct, and there is significant but lower concentration of titanium in the catalyst close to the surface,
- d) the molybdenum is clearly conferred to the catalyst.

Microprobe Results

The electron microprobe results are displayed on Figures 18A, B, and C; this figure is arranged to permit an easy comparison of the three samples for the several elements considered. Figure 18A is the top sample, 18B the middle sample and 18C the bottom sample. These elements were examined in each scan and the data are referenced to the aluminum signal. The amplitude of the signal is proportional to the line averaged concentration of the element.

Molybdenum and nickel are the active elements in the catalyst. The molybdenum signal in the crust is only slightly greater than background, and therefore there does not appear to be migration of this element. The nickel signal was amplified far more than molybdenum and therefore the signal has far more noise. Nickel is above background in the crust in 18A, B, and C and the broadened transition of the profile between the interior and the crust suggest that nickel has migrated slightly.

Iron and sulfur are found in the exterior crust of 18A and 18B and in the crust of 18C. Previous work has established that this crust is nonstoichiometric ferrous sulfide. This material appears in surprisingly large quantities in this investigation; obviously the coal-derived liquid carries all of the mineral found in coal. On the other hand in the interior the iron signal decays to background level within 125 microns of the surface while the sulfur stabilizes on the value appropriate to the sulfided catalyst.

Whenever there is a void in the catalyst (18B has a clear example) the aluminum and sulfur signal will decrease together.

Titanium, calcium and silicon are elements found in the mineral matter of coal. The titanium signal in 18A and 18B shows clearly the inner crust; the concentration of titanium in the inner crust is about twice as high as in the exterior crust of 18A and 18B or the outer crust of 18C. Thus the laydown of the inner crust appears to occur by a different mechanism than the outer crust. There is a surprisingly large penetration of titanium into the interior of the catalyst. The decoration of cracks and voids with titanium is seen as an irregular but diminishing penetration of titanium into the catalyst interior.

Silicon is a major component in the outer crust of 18A and B and in the crust of 18C. Further there is a substantial penetration of this element into the catalyst interior. Since silicon is found in the cracks near the surface, it is apparent that the catalyst is spalling away by interactions of the mineral matter. Calcium, on the other hand, has only a very weak signal in the interior of the catalyst. Further calcium and silicon apparently exclude each other in the surface crust and interior deposition.

The zinc signal shows the deposition of very low quantities of this material near the catalyst surface, particularly in the top sample. Thus the catalyst appears more active for deposition in the early part of the run; this activity is lost down the reactor.

These microprobe results are consistent with the SEM and electron microprobe area scans. The inner crust is a real phenomena, and the refractory components of the clay mineral matter are small enough to penetrate a significant way into the catalyst. FeS_x remains in the feed slurry and becomes firmly attached to the catalyst exterior. These deposits diminish the extent to which the catalyst can be regenerated.

Plasma Etched Samples

Figures 19A and 19B are two magnifications of a catalyst sample which has been plasma etched to remove oxidizable material "coke" and then reveal the firmly attached exterior crust. Figure 18A shows two cleavage planes through the catalyst and the irregular surface at the left of the picture. The exterior surface is covered with waves of deposited material. Figure 18B shows the marked rectangle on 18A at higher magnification. The surface contains aggregates of crystalline material with an 0.5 to 2.0 micron crystal size. (The largest crystal in the figure was used as a marker. This crystal appears to be a chip held to the surface electrostatically.)

Figure 20B is a view along the transverse axis of a pellet cleaved on the radial plane. The sample was taken from the bottom of the reactor where the external crust is irregular. After plasma etching no residual crust was found. However the radial plane is dotted with round pits and plateaus which have been observed in all of the polished sections. The pits near the

surface occasionally are partially filled with deposited mineral matter. Further the exterior surface of the catalyst has eroded to become quite rough. This micrograph shows that the round pits seen in all of the micrographs are not an artifact of sample preparation.

Catalyst Activity Results

A total of eight experimental runs were conducted. Table IV presents the catalysts used in each run. Two of the runs were blank runs to determine the background activity of the reactor. The fresh, spent and regenerated catalysts were used in two different sizes comprising of the other six runs. All experiments were conducted at the same operating conditions presented in Table III. However the duration of the runs varied.

Figures 21 and 22 show the total nitrogen removal and the total sulfur removal for crushed catalyst run in the fresh, spent and regenerated states. These figures show that these reactions follow pseudo first-order kinetics over limited ranges of element removal. Equivalent plots are obtained for runs made with the three states of pelleted catalysts.

Table V presents the first-order rate parameters corrected for background activity. This table shows that the pelleted catalysts have either equal or larger activities than the corresponding crushed catalyst; these results are contrary to the usual effect of isothermal transport limitations in catalysts. These results will be described more fully below.

Figure 23 shows the network for the hydrogenolysis of quinoline developed by Shih et al. (4). The individual rate constants for this network are obtained as pseudo first-order rate parameters using the techniques developed by Himmelblau et al. (5). The experimental data were analyzed using three different weighting schemes and the best weighting scheme was chosen based on the overall fit of the data and the reduction of the sum square error. Figures 24 and 25 show a comparison of the data with the parametric representation. These figures show reasonable agreement between the model and the data; the pseudo first-order form provides a simple and adequate representation of the network.

The individual rate parameters for this network analysis, corrected for background reactivity, are presented in Table VI. The rate parameters for pellets are lower than those for crushed catalyst in the three states, fresh, spent and regenerated for all parameters except k_6 . The parameter k_6 governs the conversion of 1,2,3,4-tetrahydroquinoline to orthopropylaniline; the rate parameter for subsequent step for nitrogen removal cannot be obtained reliably from the data, and thus this step represents an apparent dead end for nitrogen removal. Hence it is useful to calculate the concentration of all intermediate nitrogen compounds using the parameters of the reaction network.

Figure 26 compares the data for total nitrogen concentration with the values predicted by the model for fresh crushed catalyst; the model represents the data adequately. Similar comparisons

were made with the other five cases, and the experimental data are represented with equivalent acceptability. Thus the network representation is consistent with the overall rate of nitrogen removal for all cases.

There is direct evidence that some of the reaction rates in pellets are inhibited by transport considerations. Figure 27 shows the 1,2,3,4-tetrahydroquinoline (1THQ) and quinoline concentrations as a function of time for fresh crushed and pellet catalysts runs under otherwise identical conditions. Consistent with the lower forward apparent rate parameter for the reversible reaction, the pellet data show a higher concentration of quinoline, a lower concentration of 1THQ, than for crushed catalyst. In addition the maximum in the 1THQ concentration occurs earlier for the crushed catalyst than for the pelleted run. Therefore the pellets exhibit direct evidence for transport limitations in the catalyst.

The utility of this assumption can be tested by calculating the effectiveness factor for the pellet catalyst based upon the crushed catalyst parameters. This calculation assumes that the crushed catalyst is small enough to give intrinsic rates for all rates; this assumption can be examined later. Table VII outlines the results of the calculation.

The parameter values for the pellet catalyst agree reasonably well with the calculated values; the exceptions are k_6 and k_8 .

A similar calculation for the regenerated (Table VIII) catalyst shows that again with the exception of k_6 the calculated values for the pellet catalyst are too high in comparison to the data.

The low values found for the pellets show that there is a significant loss in the effective diffusivity for the pellets. This loss is the result of deposition of mineral matter on the exterior of the pellets; this transport resistance is removed (or avoided) when the regenerated catalyst is crushed.

Table IX gives the percentage activity remaining in the five catalyst forms relative to fresh crushed catalyst. The values observed stem from several causes: 1) intrinsic loss in kinetic activity, thus the spent catalyst has about 3-4 percent of the fresh catalyst activity and the regenerated catalyst has circa 60 percent of the original activity; 2) internal diffusional transport losses; 3) contributions from the external and near surface mineral material on the pellets, and 4) an abnormal enhancement of the k_6 and k_8 rate parameters in pellets. With reference to the latter, Bhide (6) has shown that the hydrogenolysis rate has the approximate form $\text{rate} = kKC/(1+KC)^2$, where C is the reactant concentration and K is the adsorption term. This rate expression is negative order for KC greater than one, and thus a decreasing concentration profile to the center of the pellet will increase the effective reaction rate. Thus the enhanced overall rate for HDN in pellets is in part the result of coupling transport limitations with the very strong adsorption equilibrium of nitrogen hetrocycles.

The reaction network shown in Figure 28 for dibenzothiophene hydrodesulfurization has been determined earlier by Houalla *et al.* (7). However, their reaction network was determined using only dibenzothiophene as a reactant. In this study, dibenzothiophene and biphenyl were observed for the crushed particles, and runs using pellets contained traces of cyclohexyl benzene in addition to the above two products. Concentration profiles suggested that cyclohexyl benzene is a secondary product. Bhide (6) found that quinoline inhibits the hydrogenation steps in the dibenzothiophene network strongly, and in our experiments the concentration of quinoline was very high.

Based on all the above information the dibenzothiophene HDS data were analyzed using the following network:

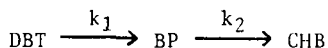


Table VIII presents the individual rate constants. The table shows that spent catalyst had a very low activity. However, unlike nitrogen removal, the spent catalyst is not totally non-reactive. For fresh catalyst the pellets are significantly more active than crushed pellets. Further cyclohexyl benzene, a hydrogenated product from biphenyl, was found only in the pellet runs. Broderick (8) and Sapre (9) have studied biphenyl hydrogenation and have shown that biphenyl hydrogenation is extremely slow and is severely inhibited by the presence of quinoline. This observation can be explained in terms of transport limitations in pellet runs in two

different ways. Since transport limitations exist in the case of pellets, the biphenyl concentration will probably be higher in the interior of the catalyst particles than for crushed catalyst. The higher concentration of biphenyl and the significantly longer residence time in the catalyst couple to increase the probability of formation of cyclohexylbenzene. The concentration profile for nitrogen hetrocycles in the catalyst interior also contributes to the observed difference between pellets and crushed catalysts. The catalyst pellets have a lower interior concentration of quinoline and THQ as opposed to the crushed particles, and hence the inhibiting effects of quinoline on dibenzothiophene is lower in the case of pellets. Thus the interior reactivity is higher for pellets, but the overall rate is lower than would be observed if quinoline were absent.

Discussion

The photomicrograph data provides detailed information on the deactivation of catalyst and an opportunity to compare the hydroprocessing of a coal-derived liquid with the hydroprocessing of coal. These data supplement the results from the activity studies.

The one percent suspended minerals in the feed is very significant in the deactivation of the catalyst. These suspended material are very finely divided and therefore can penetrate rather easily into the interior of the catalyst. Hence silicon, which is a major constituent of the clays in coal, is found in the interior 100 microns of the catalyst in all three samples.

This observation is consistent with the behavior of coal hydro-processing experiments.

The catalyst is deactivated by the laydown of coke. The plasma etching experiments show that the exterior crust is largely coke, and regeneration by burning decreases the sample weight by twenty percent. Thus a significant fraction of the activity can be regained by burning away the coke deposits as evidenced by the results from activity studies, however the deposited mineral matter remains.

The exterior crust also contains FeS_x ; previous studies have shown that these deposits are $\text{FeS}_{1.1}$. The crystal size of FeS_x is smaller in this system than for the synthoil catalyst. There is no evidence that the FeS_x was formed in the trickle-bed reactor; the weak penetration of iron into the catalyst correlates with the penetration of silicon, and it therefore appears that FeS_x is cemented on the catalyst with coke.

The nickel profiles indicate a small migration of this element away from the catalyst support into the crust on the surface. The migration of this promoter may affect catalyst function; in particular the effect of nickel upon the rate of coking may change.

The most unique feature of these studies is the formation of the titanium-rich inner crust on the top and middle catalyst samples.

Spent catalyst was found to be essentially non-reactive for both sulfur and nitrogen removal. Network analysis for quinoline HDN and dibenzothiophene HDS indicate that the laydown of coke seems to affect both hydrogenation and bond-breaking steps in the same way. The results from the experiments using the regenerated catalysts show that half of the activity was recovered by the regeneration process. A comparison of the runs using catalyst pellets and crushed particles shows that the catalyst interior is filled with coke and inactive. These results also raise some interesting questions on the interplay between diffusion limitations and the interactions between nitrogen and sulfur-containing compounds upon the intrinsic kinetics.

The results presented here are similar to the ones observed from characterization studies performed on catalysts that have been in direct contact with coal, except for a few minor differences.

Since 50 to 60 percent of the catalyst activity can be recovered by burning the coke, the mineral matter is secondary in the direct deactivation of the catalyst. However, the deposited mineral matter is a potential catalyst for coke formation; thus the effective lifetime for the regenerated catalyst may be less than that for a fresh catalyst.

Acknowledgements

This work was supported by a grant from the Department of Energy.

Literature Cited

1. Stanulonis, J. J., Gates, B. C., and Olson, J. H., AICHE J., 22, 576 (1976).
2. Chiou, M. J. and Olson, J. H., Am. Chem. Soc., Div. Pet. Chem., Prepr., 23 (4), 1421 (1978)
3. Chiou, M. J. and Olson, J. H., 'Catalyst Deactivation in Coal Liquefaction Processes,' submitted to AICHE J.
4. Shih, S. S., Katzer, J. R., Kwart, H., and Stiles, A. B., Am. Chem. Soc.; Div. Pet. Chem. Prepr., 22(3), 919 (1977).
5. Himmelblau, P. M., Jones, C. R., and Bischoff, K. B., Ind. Eng. Chem. Fundam. 6, 539 (1967).
6. Bhide, M., Ph.D. Thesis, University of Delaware, 1979.
7. Houalla, M., Nag, N. K., Sapre, A. V., Broderick, D. H., and Gates, B. C., AICHE J. 24, 1015 (1978).
8. Broderick, D. H., Ph.D. Thesis, University of Delaware, 1979.
9. Sapre, A. V., Ph.D. Thesis, University of Delaware, in preparation.

TABLE I

Feed Oil PropertiesEqual Volume Mixture of Raw Anthracene Oil and
Synthoil Liquid

Carbon, wt %	84.92
Hydrogen, wt %	6.57
Sulfur, wt %	0.54
Nitrogen, wt %	1.21
Ash, wt %	1.05

TABLE II

Operating Conditions in the Trickle-Flow Reactor

Temperature -	371°C
Pressure -	.1500 psig
Liquid Volume Hourly Space Time -	1.25 hrs
H ₂ /Oil Ratio -	7500 scf/bbl
Run Duration -	674 hours

TABLE III

Operating Conditions in Batch Autoclave Reactor

Temperature -	350°C
Pressure -	36 atm
Catalyst Concentration -	0.5 wt %
CS ₂ Concentration -	0.05 wt %
Carrier Oil -	Hexadecane
Quinoline Concentration -	2 wt %
Dibenzothiophene Concentration -	1 wt %

TABLE IV

Catalysts Used in Batch Experimental Runs

<u>Run No.</u>	<u>Catalyst Used</u>	<u>Catalyst Size</u>	<u>Duration, minutes</u>
1	Fresh	140 mesh	600
2	Spent	140 mesh	1280
3	Regenerated	140 mesh	1260
4	Fresh	8/10 mesh	1200
5	Spent	8/10 mesh	1800
6	Regenerated	8/10 mesh	1250
7	Blank run without boat		600
8	Blank run with boat		2500

TABLE V

Total Nitrogen and Sulfur Removal
Pseudo First Order Rate Constants, $\frac{\text{g of oil}}{\text{g of cat. minutes}}$

	<u>Fresh</u>		<u>Spent</u>		<u>Regenerated</u>	
	C	P	C	P	C	P
Nitrogen	0.195	0.214	0	0	0.116	0.165
Sulfur	0.333	0.491	0.333	0.222	0.168	0.165

TABLE VI

Individual Reaction Rate Constants
for the Quinoline Network, $\frac{\text{g of oil}}{\text{g of cat. minutes}}$

	<u>Fresh</u>		<u>Spent</u>		<u>Regenerated</u>	
	C	P	C	P	C	P
k ₁	81.19	9.045	0.908	0	46.07	3.566
k ₂	12.92	1.835	0.135	0	10.96	0.620
k ₃	1.120	0.676	---	0.042	0.627	0.216
k ₄	0.167	0.114	0.0042	0	0.153	0.121
k ₅	0.727	0.422	---	0	0.182	0.025
k ₆	0.101	0.218	0.0042	0	0.064	0.107
k ₇	---	---	---	0	---	---
k ₈	1.752	1.66	0	0	1.372	0.170

TABLE VII

Theoretical Calculation of Rate Parameters for Fresh Pellets

	<u>Crushed Rate</u> <u>g oil/g cat min)</u>	<u>Thiele Modulus</u>	<u>η</u>	<u>P_{cal.}</u>	<u>P_{found}</u>
k ₁	81.19	13.51	0.074	9.27	9.045
k ₂	12.92	5.39	0.185	2.39	1.83
k ₃	1.12	1.59	0.58	0.65	0.68
k ₄	0.167	0.61	0.89	0.15	0.11
k ₅	0.727	1.28	0.67	0.49	0.422
k ₆	0.101	0.48	0.93	0.093	0.218
k ₈	1.752	1.98	0.49	0.85	1.66

TABLE VIII

Theoretical Calculation of Rate Parameters
for Regenerated Pellets

	<u>Crushed Rate</u> <u>(g oil/g cat·min)</u>	<u>Thiele</u>	<u>n</u>	<u>P_{calc}</u>	<u>P_{found}</u>
k ₁	46.1	10.18	0.098	4.53	3.57
k ₂	11.0	4.97	0.20	2.21	0.62
k ₃	0.63	1.19	0.70	0.44	0.22
k ₄	0.15	0.587	0.90	0.134	0.121
k ₅	0.18	0.637	0.88	0.16	0.025
k ₆	0.064	0.40	0.95	0.058	0.107
k ₈	1.372	1.76	0.53	0.74	0.170

TABLE IX

Rate Constants in the Quinoline NetworkRelative to Fresh Catalyst, %

	k_1	k_2	k_3	k_4	k_5	k_6	k_7	k_8
Spent pellets	0	0	6	0	0	0	--	0
Spent particles	1	1	0	3	0	4	--	0
Regenerated Pellets	39	33	32	100	6	49	--	10
Regenerated particles	57	85	56	92	25	63	--	78

TABLE X

Individual Rate Constants for
 Dibenzothiophene Hydrodesulfurization, $\frac{\text{g of oil}}{\text{g of cat} \cdot \text{minutes}}$

	Fresh		Spent		Regenerated	
	C	P	C	P	C	P
k_1	0.333	0.491	0.033	0.022	0.168	0.165
k_2	---	0.008	---	---	---	0.007



LIST OF FIGURES

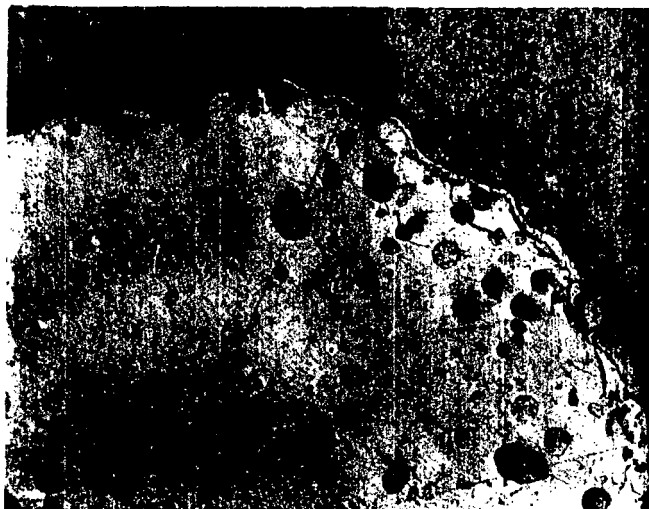
Figure

- 1 Light microscopy of top sample A. 100x; B. 200x.
- 2 SEM top sample A. backscatter electron; B. aluminum EDAX.
- 3 SEM-EDAX of top sample A. silicon; B. calcium.
- 4 SEM-EDAX of top sample A. sulfur; B. iron.
- 5 SEM-EDAX of top sample A. titanium; B. molybdenum.
- 6 Microprobe area scans A. backscatter electron;
B. titanium.
- 7 Light microscopy of middle sample A. 100x; B. 200x.
- 8 SEM of middle sample A. 400x; B. 800x.
- 9 SEM-EDAX of middle sample A. silicon; B. calcium.
- 10 SEM-EDAX of middle sample A. sulfur; B. iron.
- 11 SEM-EDAX of middle sample A. titanium; B. molybdenum.
- 12 Light microscopy of bottom sample A. 100x; B. 200x.
- 13 SEM of bottom sample A. 200x; B. 400x.
- 14 SEM of interior spot A. backscatter electron;
B. ground current.
- 15 SEM-EDAX of bottom sample A. silicon; B. calcium.
- 16 SEM-EDAX of bottom sample A. sulfur; B. iron.
- 17 SEM-EDAX of bottom sample A. titanium; B. molybdenum.
- 18 Electron microprobe results for the three samples
A. top; B. middle; C. bottom.
- 19 SEM of plasma etched surface of top sample A. 200x;
B. 2000x.
- 20 SEM of plasma etched surfaces A. 200x middle sample;
B. 100x bottom sample.
- 21 Comparison of total nitrogen removal for fresh, spent
and regenerated catalysts.

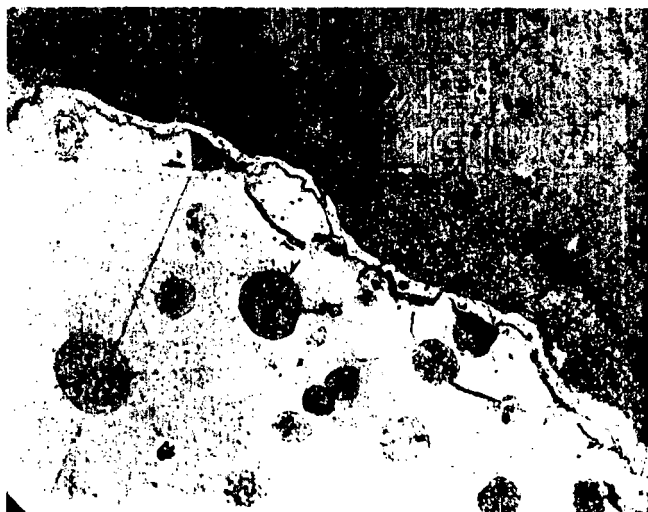
Figure

- 22 Comparison of total sulfur removal for fresh, spent and regenerated catalysts.
- 23 Network for quinoline hydrodenitrogenation.
- 24 Comparison of experimental data and predicted values for quinoline and 1,2,3,4-tetrahydroquinoline concentrations.
- 25 Comparison of experimental data and predicted values for orthopropylaniline, 5,6,7,8-tetrahydroquinoline and decahydroquinoline concentrations.
- 26 Comparison of experimental data and predicted values for total nitrogen removal for fresh catalysts.
- 27 Effect of catalyst particle size on quinoline and 1,2,3,4-tetrahydroquinoline concentration.
- 28 Network for dibenzothiophene desulfurization.

Light Microscopy—top sample



100x



200x

Scanning Electron Microscopy - top sample



400x
Backscatter
Electron

SEM-EDAX Area Scan - top sample

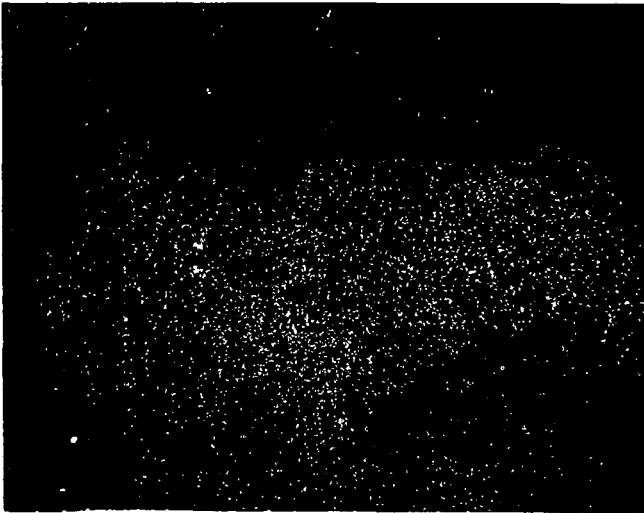


400x
Aluminum
EDAX

SEM-EDAX Area Scans - top sample

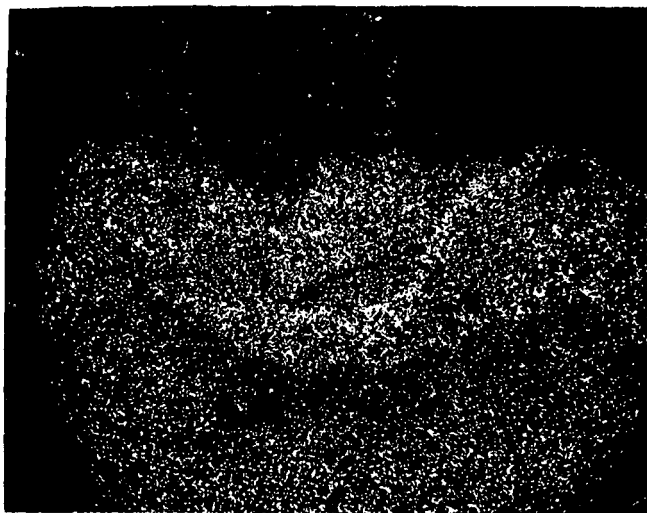


400x
Silicon

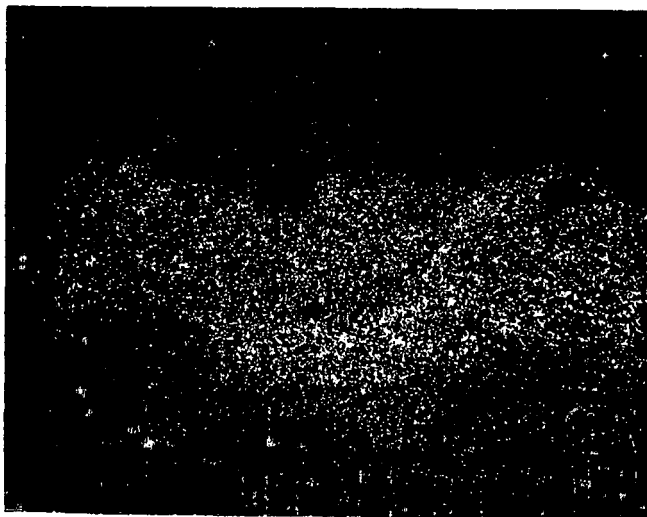


400x
Calcium

SEM-EDAX Area Scans - top sample



400x
Sulfur



400x
Iron

SEM-EDAX Area Scans - top sample



400x
Titanium

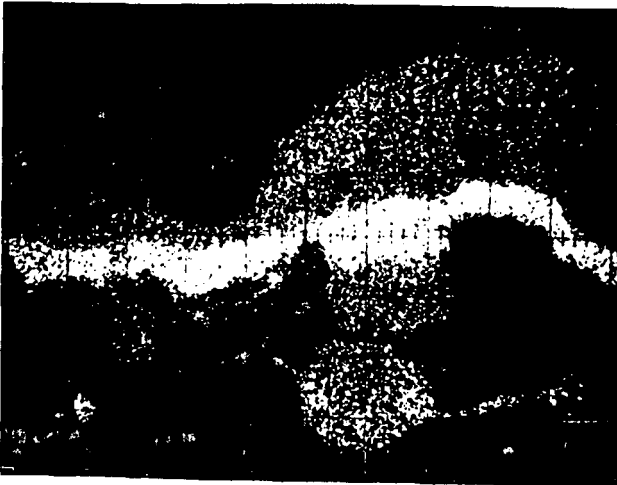


400x
Molybdenum

Microprobe Scans - top sample



500x
Backscatter
Electron



500x
Titanium

Light Microscopy – middle sample



100x



200x

Scanning, Electron Microscopy – middle sample

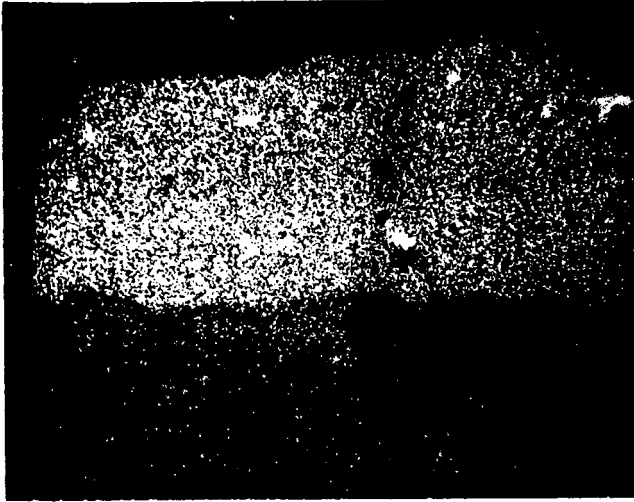


400x

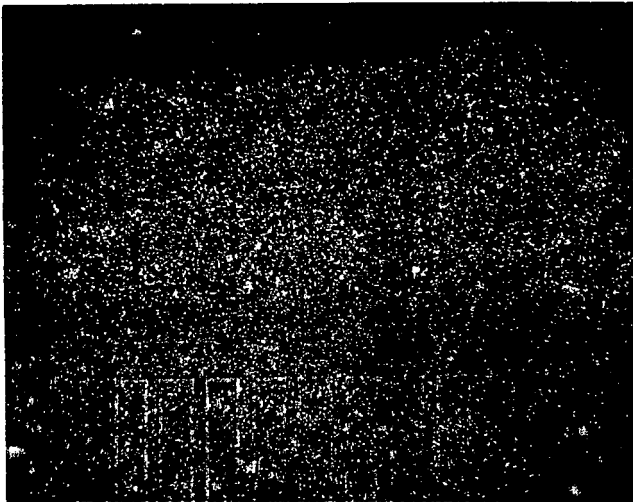


800x

SEM-EDAX - Area Scans - middle sample

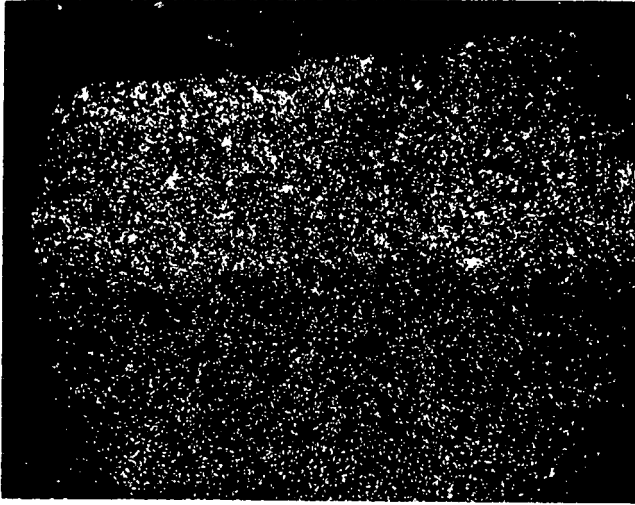


800x
Silicon

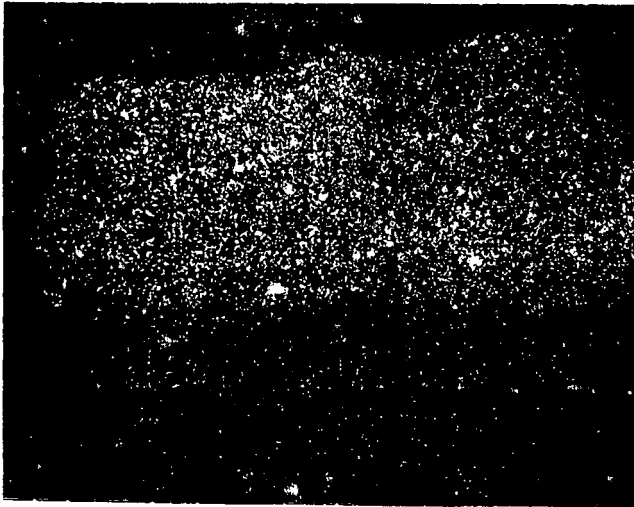


800x
Calcium

SEM-EDAX Area Scans - middle sample

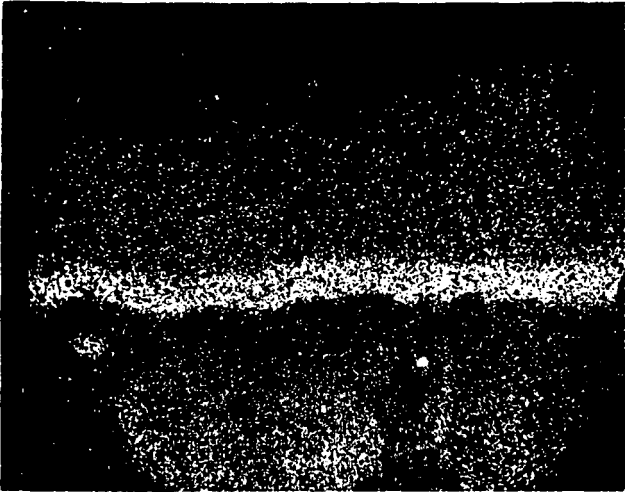


800x
Sulfur

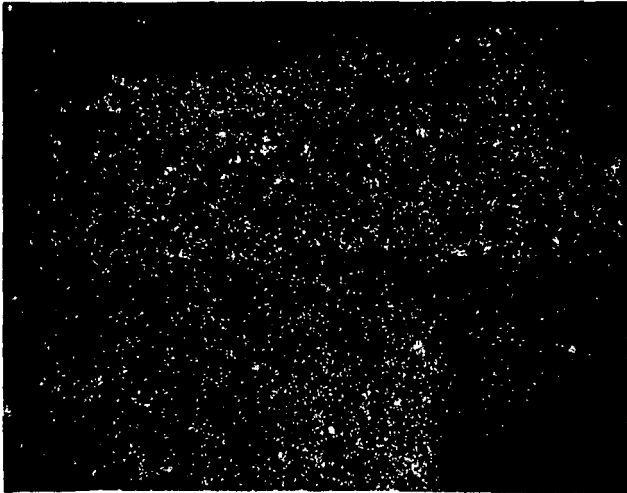


800x
Iron

SEM-EDAX Area Scans - middle sample

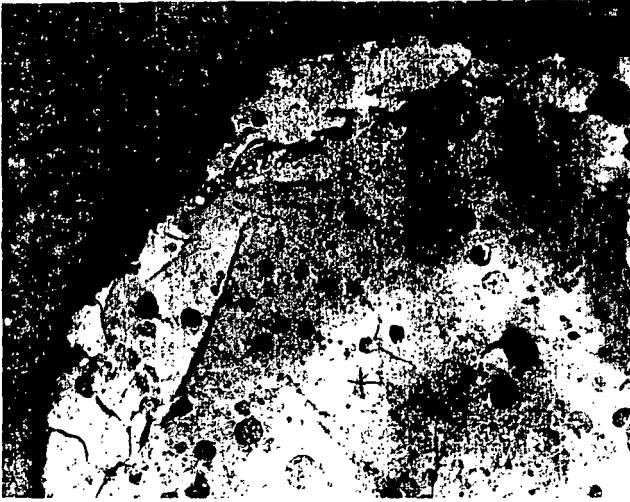


800x
Titanium

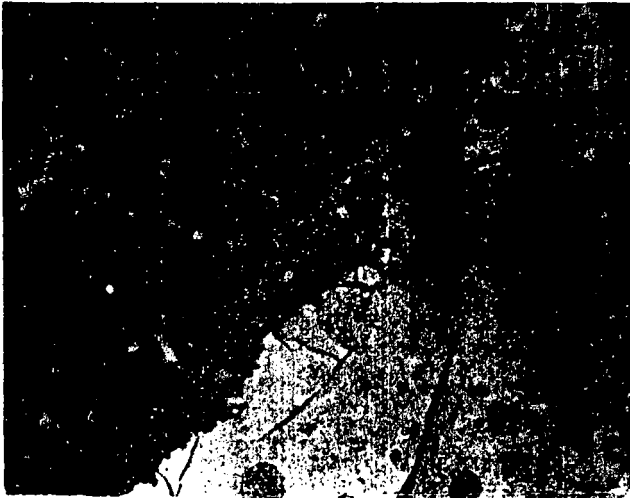


800x
Molybdenum

Light Microscopy - bottom sample

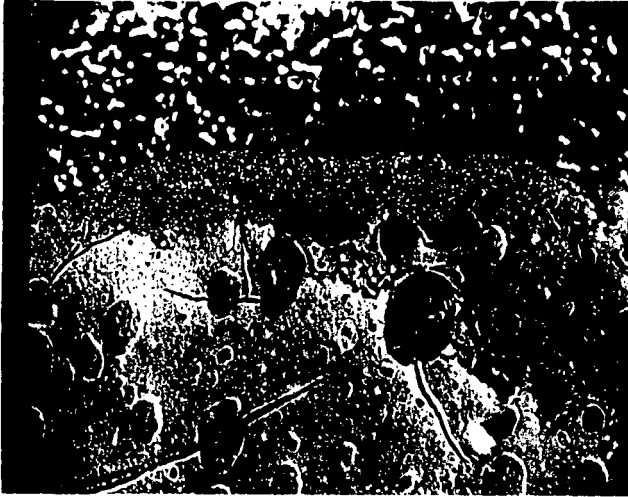


100x



200x

Scanning Electron Microscopy - bottom sample

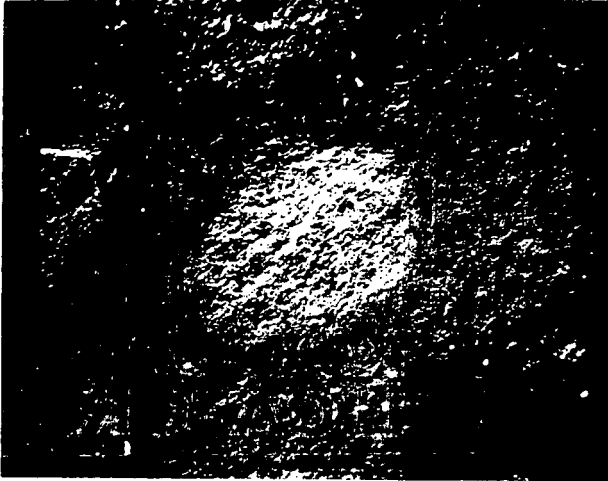


200x

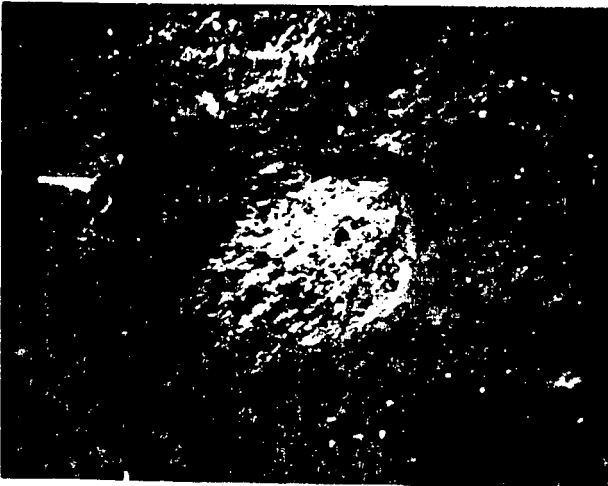


400x

Scanning Electron Microscopy
Interior Spot - 1000x, 45° tilt

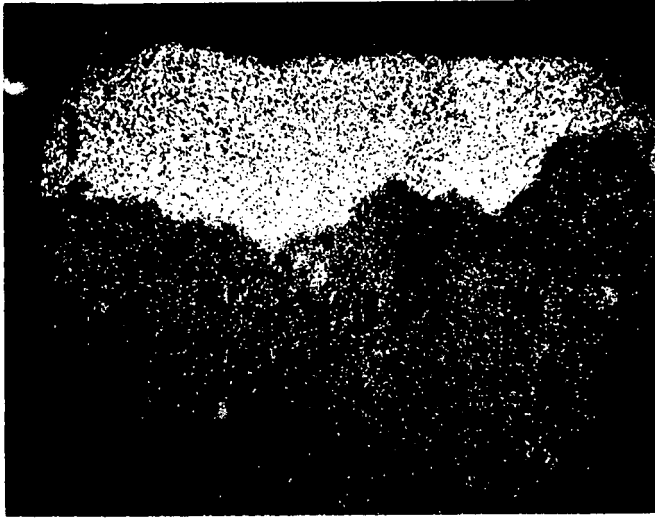


Backscatter
Electron

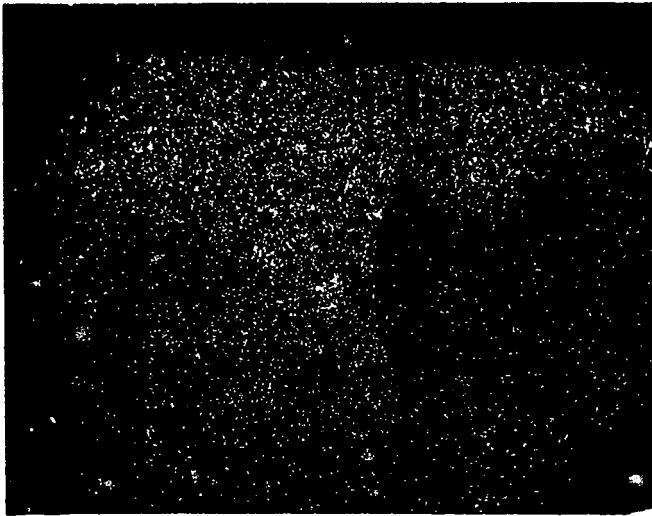


Ground
Current

SEM-EDAX Area Scans - bottom sample



400x
Silicon

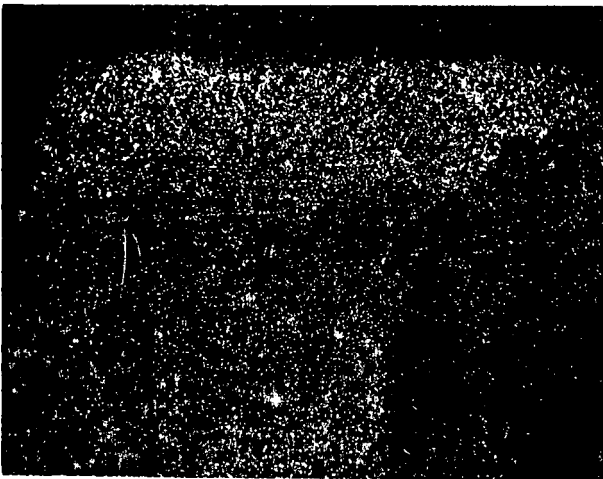


400x
Calcium

SEM-EDAX Area Scans - bottom sample

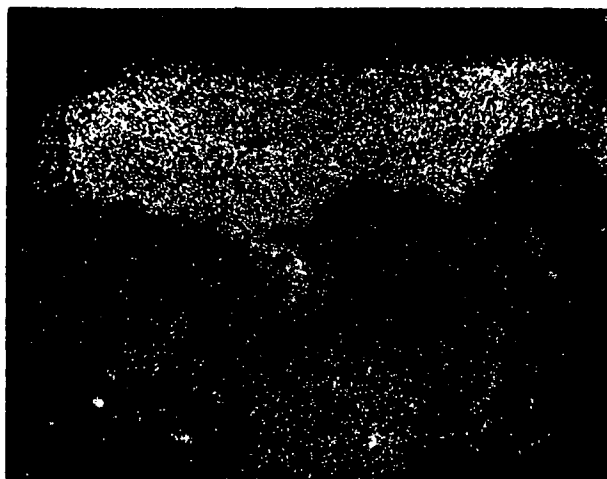


400x
Sulfur

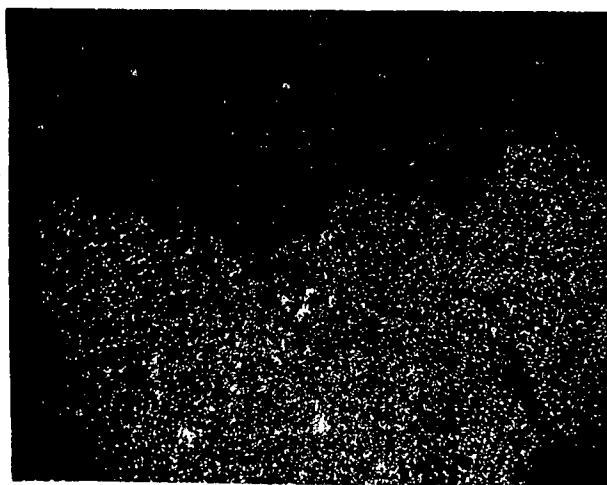


400x
Iron

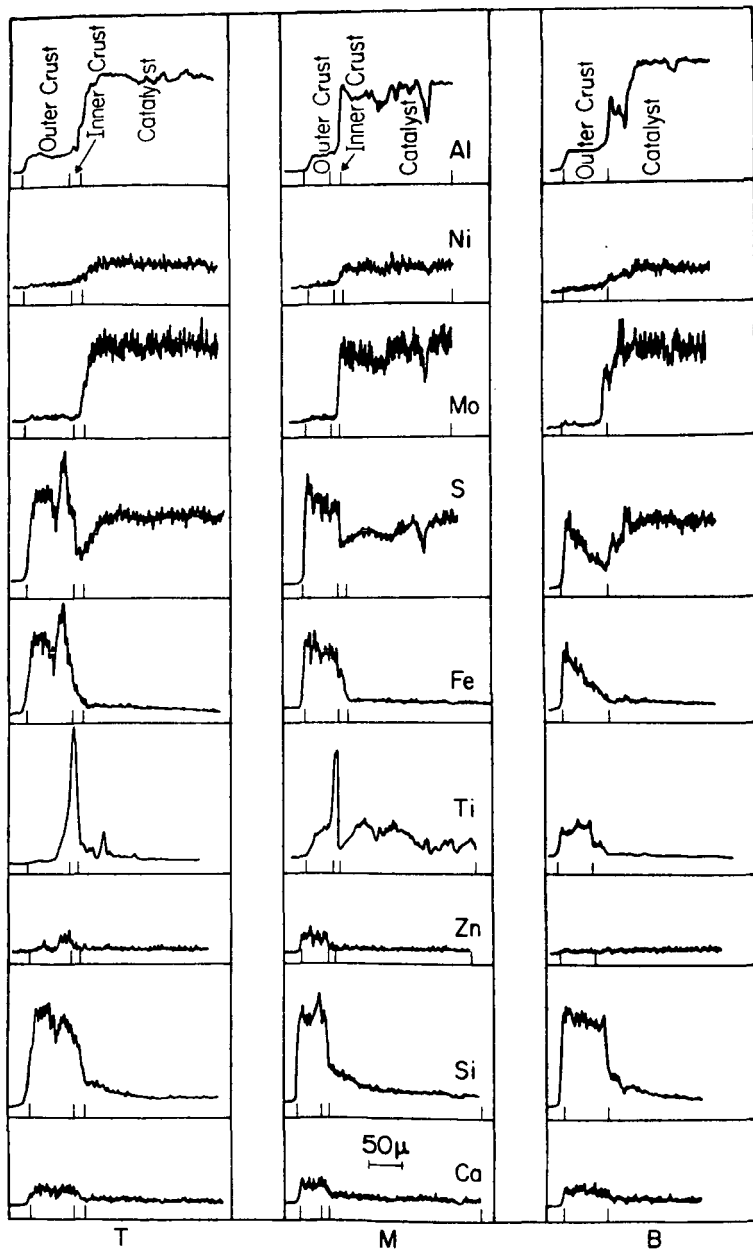
SEM-EDAX Area Scans - bottom sample



400x
Titanium

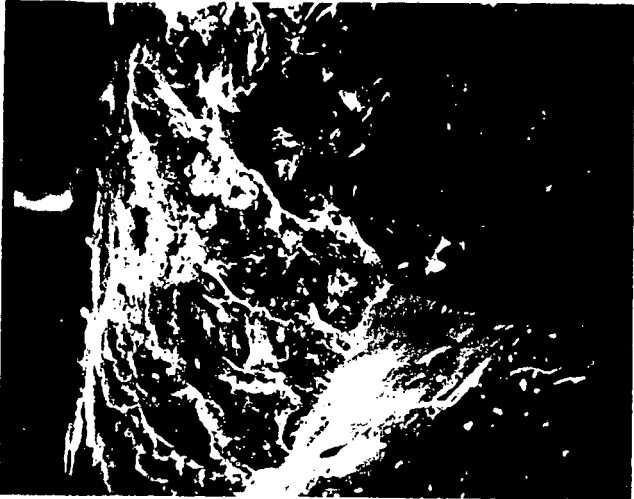


400x
Molybdenum

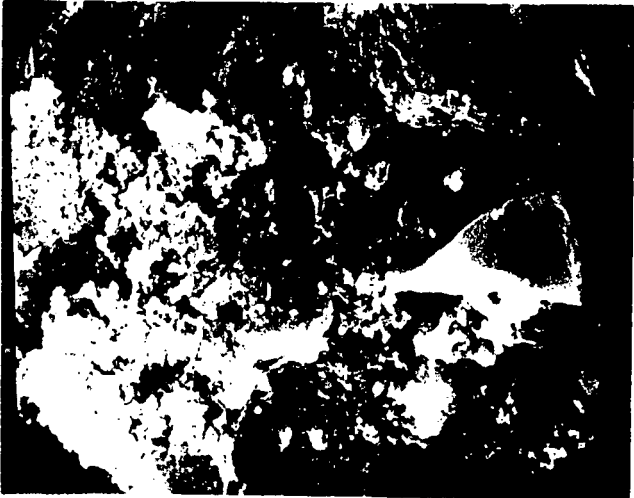


RELATIVE CONC PROFILES

SEM Plasma Etched Surface - top sample

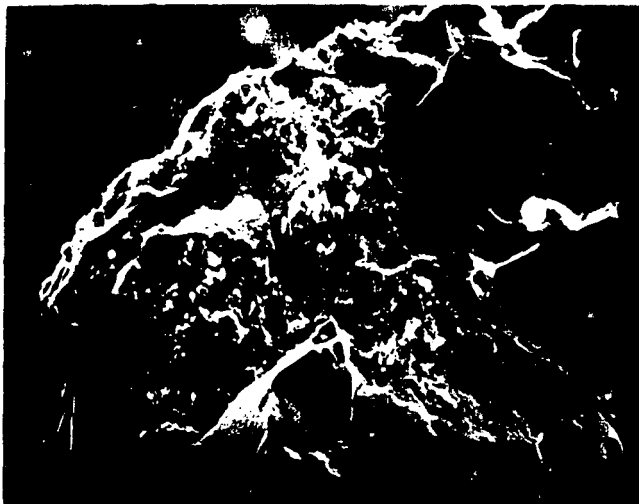


200 x



2000 x

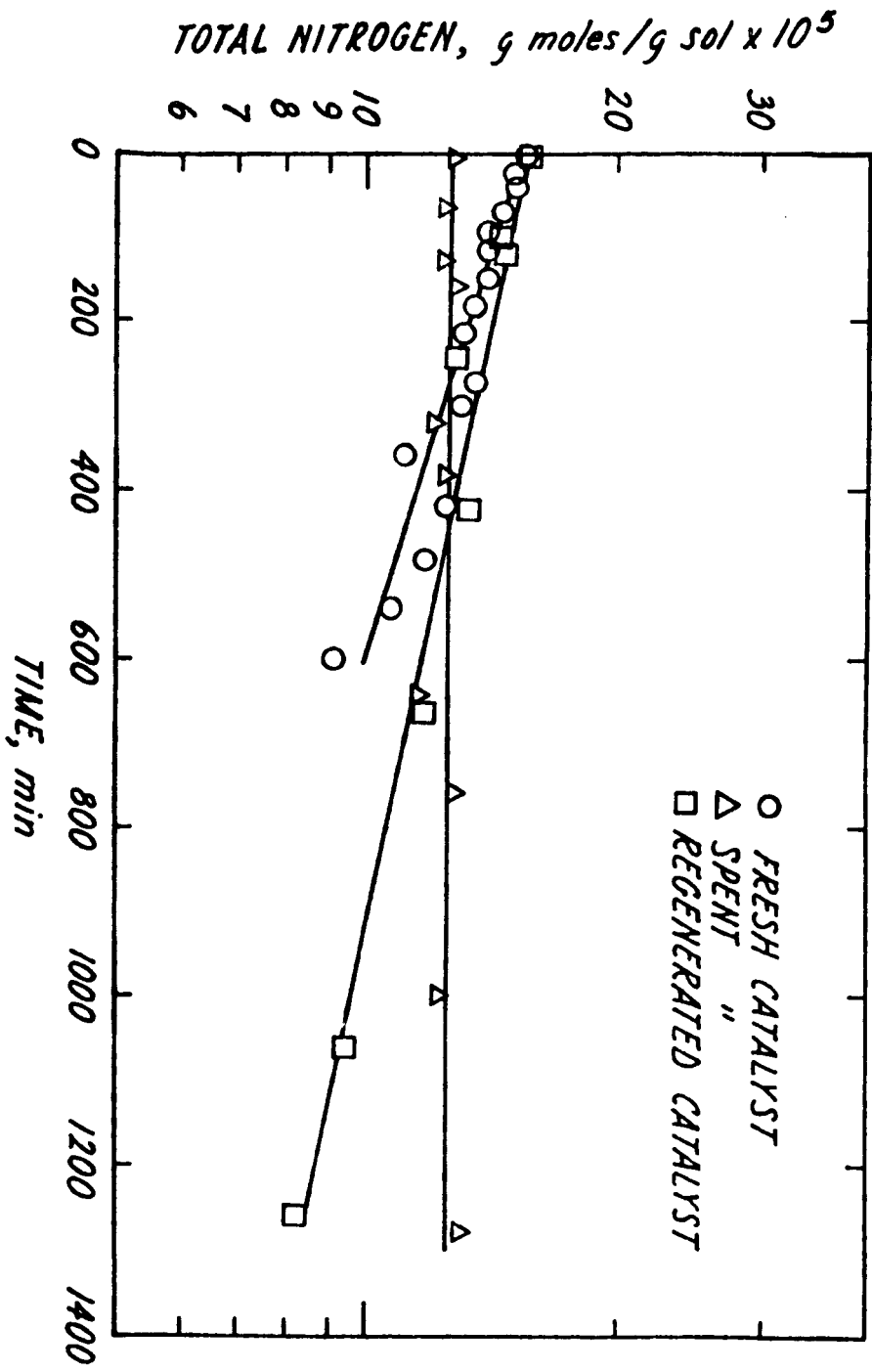
SEM Plasma Etched Surfaces



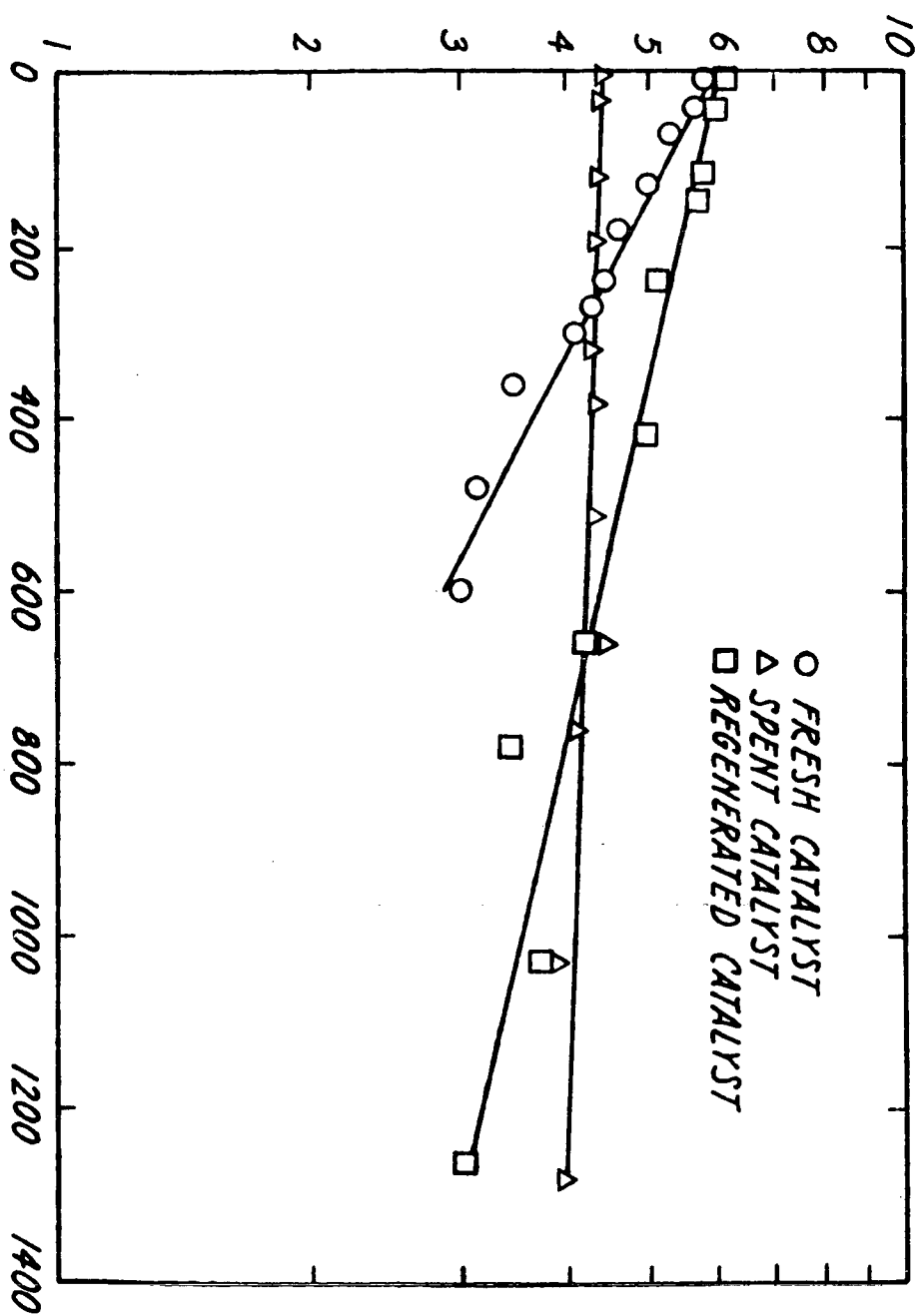
200x
Middle
Sample

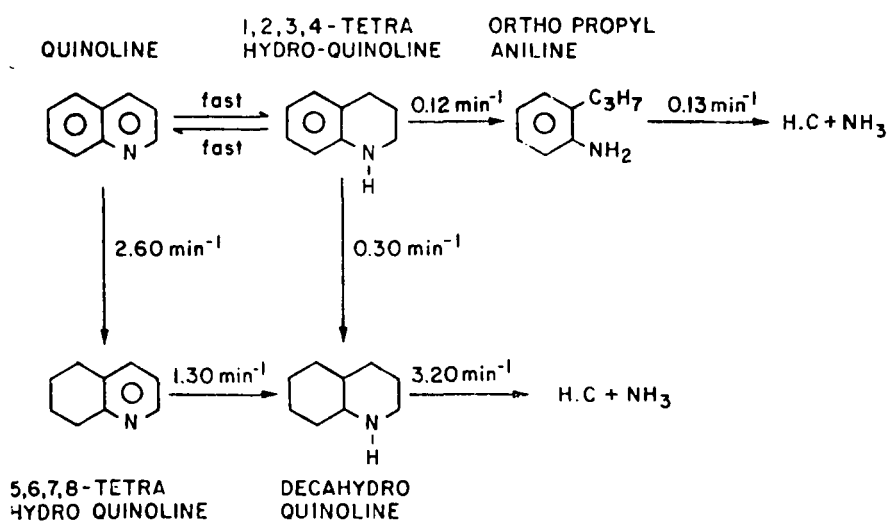


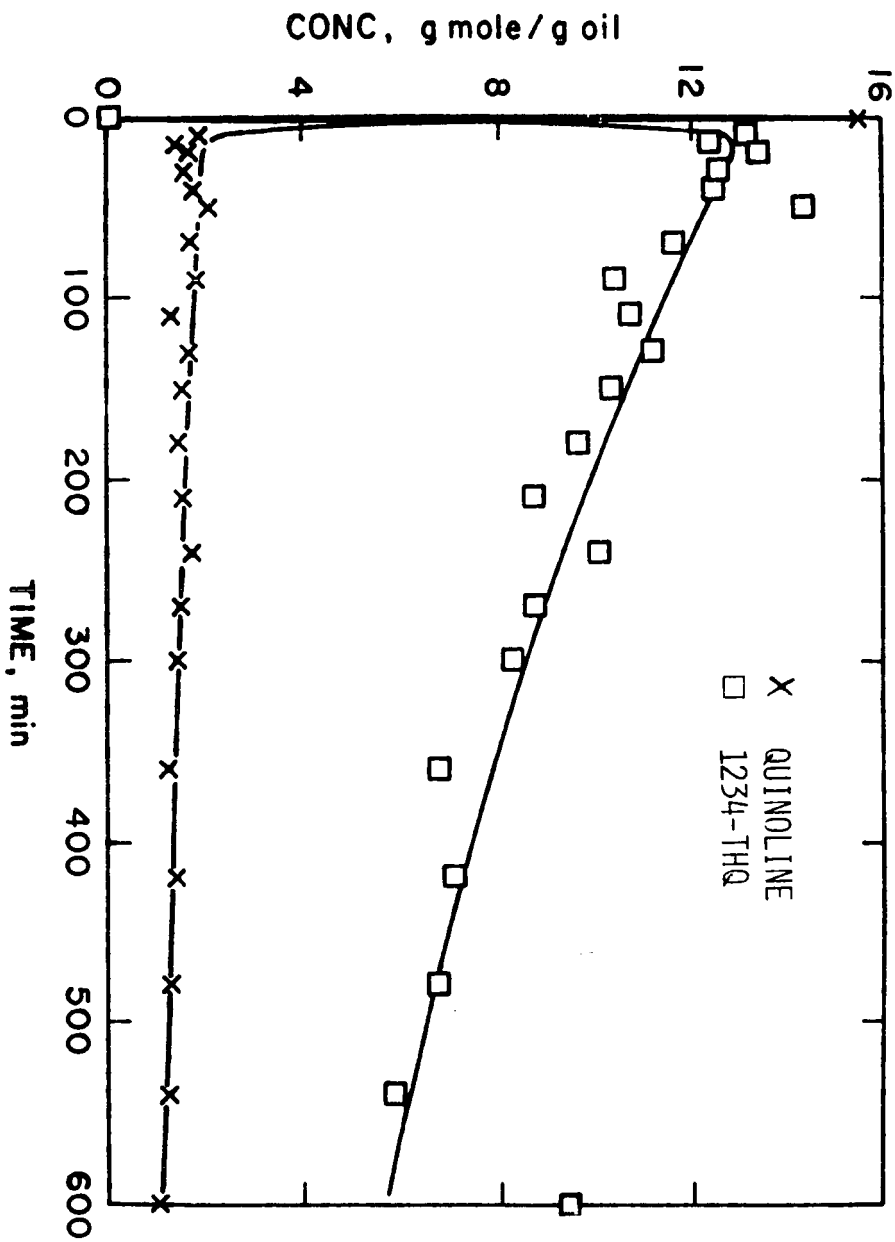
100x
Bottom
Sample

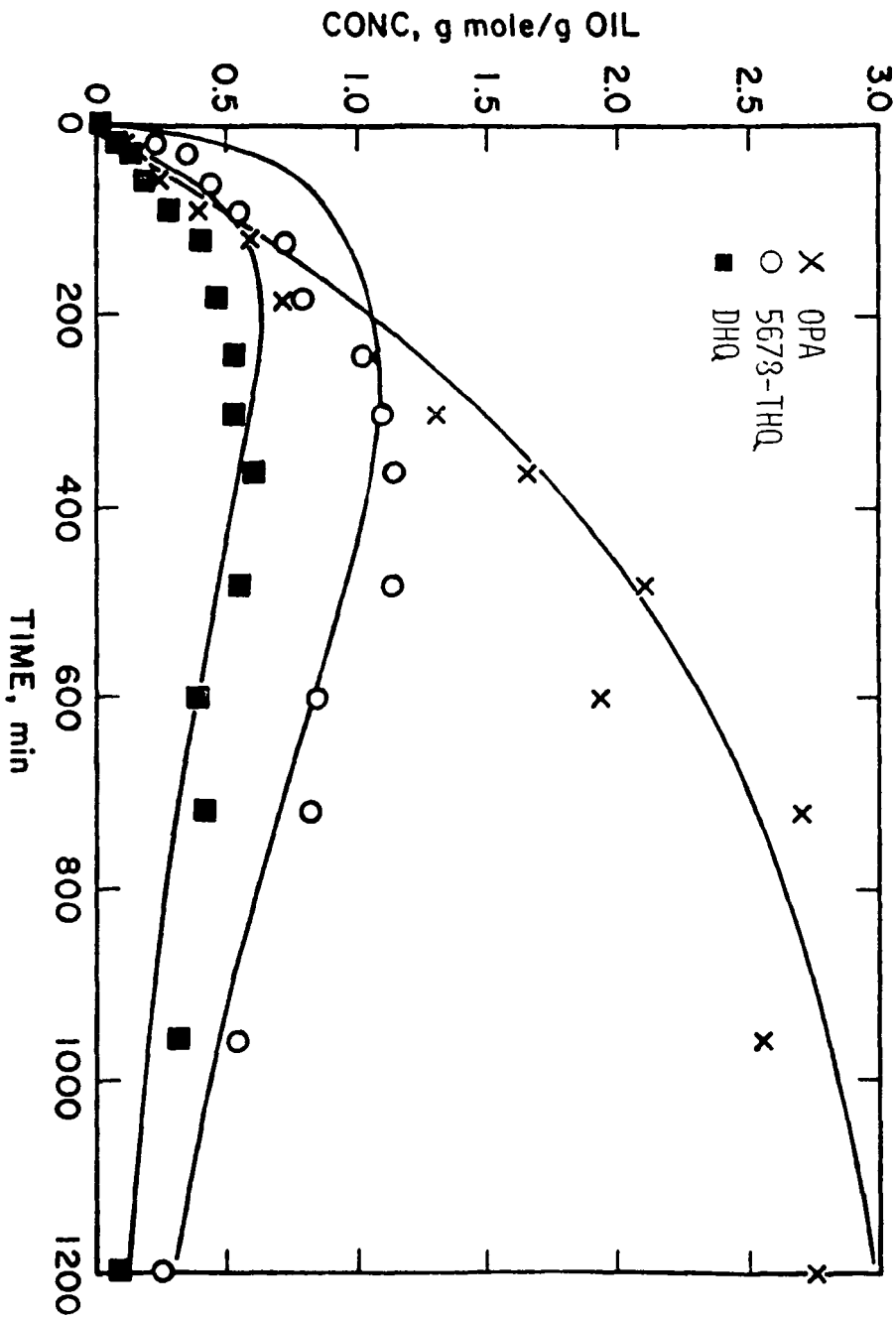


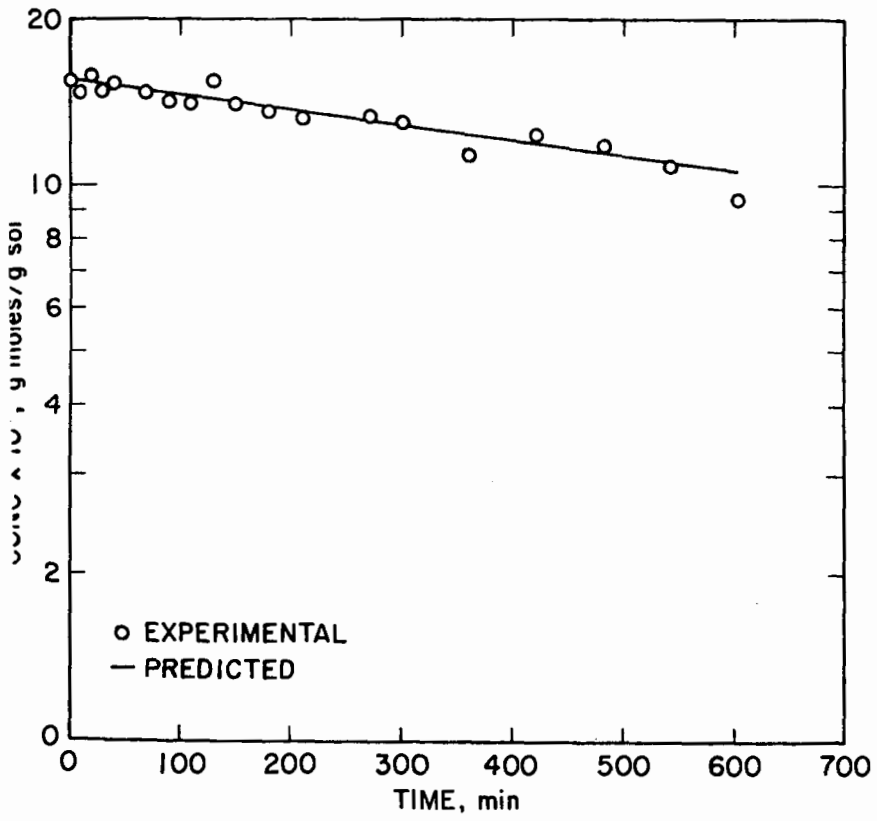
TOTAL SULFUR, g moles/g oil $\times 10^5$

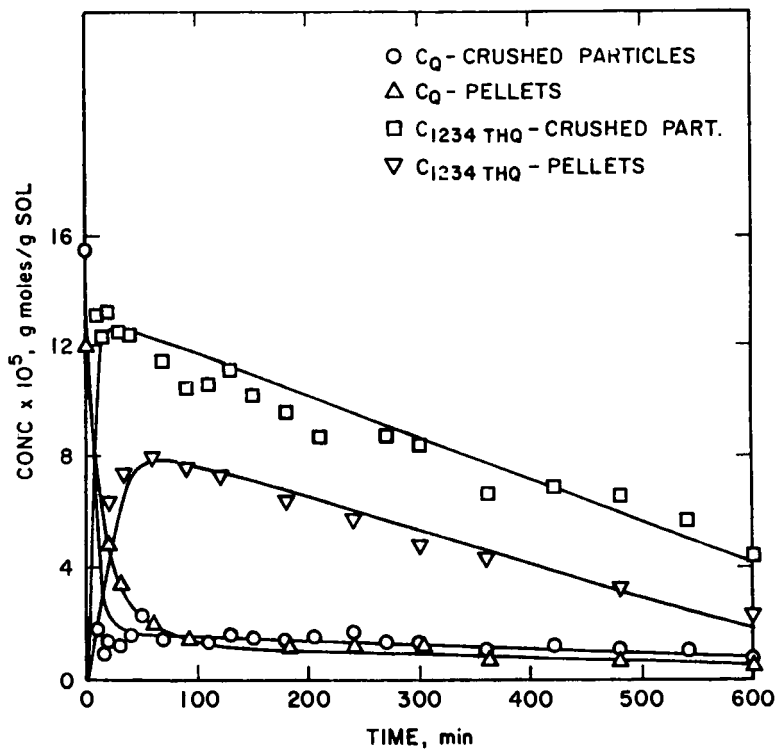


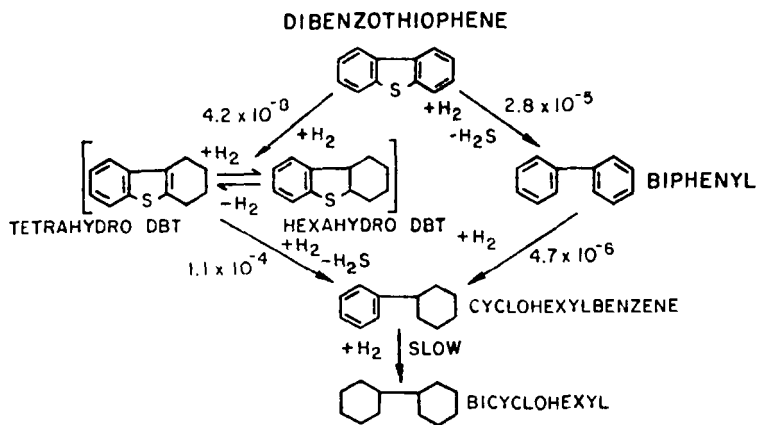












CATALYST DEACTIVATION IN HYDROTREATING COAL-DERIVED LIQUIDS by R. Sivasubramanian, J.H. Olson and J.R. Katzer. Center for Catalytic Science and Technology, Department of Chemical Engineering, University of Delaware, Newark, Delaware 19711.

Ni-Mo/Al₂O₃ catalysts aged in hydrotreating coal-derived liquids were characterized by scanning electron microscopy, electron microprobe, and catalytic activity. Aged catalyst from three different sections of the trickle-bed reactor used for the hydroprocessing were plasma etched to remove the carbon coating and were then examined. An inner crust and an outer crust were observed on the exterior of the catalyst particles; the inner crust was not present on catalyst near the reactor exit. The inner crust was composed principally of titania; whereas the outer crust contained ferrous sulfide, silica, and traces of other metals. Titania was also deposited within the interior of the catalyst. The activities of fresh, aged, and regenerated (coke burnt off) catalysts were compared for hydrodesulfurization (HDS) and hydrodenitrogenation (HDN) using a mixture of dibenzothiophene and quinoline in n-hexadecane in a batch autoclave reactor. The aged catalyst was inactive for HDN and had very low activity for HDS. Burning the carbon off the catalyst resulted in approximately 60% recovery of the HDN activity and 50% recovery of the HDS activity compared to that of the fresh catalyst. Pseudo first-order rate constants were determined for each of the reactions in the quinoline and dibenzothiophene reaction networks.